Towards real-time light source position estimation for augmented reality with an RGB-D camera

Bastiaan J. Boom[a,*], Sergio Orts-Escolano[b], Xin X. Ning[a],

Steven McDonagh[a], Peter Sandilands[a], Robert B. Fisher[a]

[a]School of Informatics, University of Edinburgh,

[b]Dpt. Computer Technology and Computation, University of Alicante,

*Email: bas_boom12@hotmail.com, bboom@inf.ed.ac.uk

Abstract

The first GPU based method for estimating a point light source position in a scene recorded by an RGB-D camera is presented. The image and depth information from the Kinect is enough to estimate a light position in a scene which allows for the rendering of synthetic objects into a scene that appear realistic enough for augmented reality purposes. This method does not require a probe object or other physical device. To make this method suitable for augmented reality, we developed a GPU implementation that performs light estimation in under one second. This is sufficient for most augmented

reality scenarios because both the position of the light source and the position of the Kinect are typically fixed. The method is able to estimate the angle of the light source with an average error of 20 degrees. By rendering synthetic objects into the recorded scene, we illustrate that this accuracy is good enough for the rendered objects to look realistic.

Keywords: Light Source Estimation, Augmented Reality, GPU implementation, RGB-D camera

Introduction

The appearance of objects in a scene depends on their illumination. In augmented reality, this illumination is often not taken into account, which makes any rendered synthetic objects look unrealistic. A Kinect sensor can obtain a depth map of the scene, enabling more realistic interactions between real objects and augmented objects [1, 2]. The goal of our work is to estimate the illuminant position in the scene based on the intensity image and depth map provided by the Kinect sensor for the purpose of improving the augmented reality experience (see Figure 1). In this paper, an estimate of the illuminant position is computed based on the Kinect's depth and intensity images without any human annotations of light sources or known objects in the scene. This work uses the Kinect, however, the techniques are not limited to this sensor and any RGB-D camera which provides a registered multispectral image and depth map allows the estimation of the illuminant in the scene.

This paper is focussed towards the application of augmented reality, although the estimation of the illuminant is applicable in multiple domains (like surface improvement, scene understanding, illumination invariant scene, etc). We have developed a methodology to estimate the location of the single point light source based on the image and the depth map provided by the Kinect, first described in [3]. In this paper, we focus on making it applicable for augmented reality, by building a GPU implementation for some of the methods using the Point Cloud Library. We show that the light source estimation can be performed in 1 second, which, in combination with other methods (like Simultaneous Localization And Mapping),

can lead to a better Augmented Reality experience.

The main contributions of this paper are:

GPU implementation of methodology: We show that it is possible to run the method introduced in [3] on a GPU, processing the incoming Kinect data with an average speed of more than 1 frame per second. This real-time implementation has potential benefits to graphics applications and game designers.

Creation of dataset: A public dataset is created to measure and verify the performance of our methodology. In this dataset, we measure the light position and angle relative to the Kinect scenes. The dataset contains multiple scenes recorded by the Kinect, where we have known positions of the light sources, the scene surface points and registered colour data. This dataset will be made publicly available after the publication (http://www.dtic.ua.es/jgpu12/lightEstimation/, password: lightEstimationEdi)

Extended experiments: New experiments are added to investigate the influence of the GPU implementation on the results. The GPU implementation requires different algorithmic choices which affect both the accuracy and speed. The two key properties that allow the presented algorithm to work are: 1) Most surfaces can be roughly approximated as Lambertian, and so the surface normals estimated from range data allow an approximate synthesis of the appearance given a light source position. In this case, the surface appearance provides partial constraints on the position of the light source. 2) Segmented surface patches based on colour and distance tend to have the same albedo.

This leads to an algorithm that, given an intensity image with associated depth and surface

normals at every point, renders images from different hypothesised light source positions and selects the position whose synthesised image best matches the original image. The algorithm can be summarised as follows:

1. Given a potential light source position, estimate the albedo at every image pixel (using the surface normal and light source position)

2. Given segmented image regions, combine the individual albedo estimates to obtain an estimated albedo for the entire surface segment

3. Using the estimated segment albedos, point surface normals and light source position, synthesise an image of the scene

4. Compute the error between the synthesised and captured real images

5. Optimize the light source position to minimize the error

Related work

In this research, we focussed on improving a part of the augmented reality experience i.e. the illumination of rendered synthetic objects in a scene. In this case, the research question is how to obtain an estimate of the light source position which can be used by rendering software. We assume that other steps necessary for the augmented reality experience, like positional tracking (e.g. Simultaneous Localization And Mapping or Parallel Tracking and

Mapping) and rendering software are available. In our literature study and the remainder of this paper, we will mainly focus on the estimation of the illuminant. This is an old research subject, where, based on the image information and often scene geometry, information about the illuminant is estimated. The approach described in [4, 5] estimates the illuminant by taking advantage of the cast shadows and specular reflections of known geometry in the scene. Extensions to this work is performed in [6] which only needs boundaries of an object and [7] which assume different reflectance models. In [8, 9], a stereo setup is used together with a probe sphere (in their case a white shiny ball) to determine multiple area light sources. The work of [10] determines the illuminant of a scene accurately using a mirror surface probe sphere to determine light maps of the scene from different exposed photographs. These light maps are a more dynamic way of modelling the illumination than assuming some synthetic light source. Augmented reality based on mirror surface probe spheres to estimate the illumination is performed by [11, 12, 13]. In Computational Color Constancy, the main interest is the color of the light source, however this often also requires some estimation of the direction (good overview papers are [14, 15]). There is work in estimating the illumination in outdoor scenes often for augmented reality without probe spheres [16, 17], using properties of sunlight and shadows. Recent work of [18] uses movement of the camera and known properties of sunlight to determine outdoor illumination conditions. Augmented reality in outdoor scenes is studied by [19, 20], where the detection of the light source in the outdoor environment is performed using GPS and compass information. A 3D sensor is used for realistic shadow rendering. Another clue to estimate the illumination in a scene is the shadow

which has been used in [21, 22]. In [23], a double camera system is used for augmented reality, where the first camera films the actual scene while a fish-eye camera is used for filming the position of the light on the ceiling. Rendering based on photographs where light sources, i.e. windows are annotated by users is performed in [12].

Recent work on this subject by [24, 25], try to decompose the RGB-D input into albedo and shading fields in order to explain the scene. Other work focusses on using the light estimates for shape from shading to improve the depth maps given by the RGB-D cameras [26]. Our work [3] focusses more on using the illuminant estimation in augmented reality, where computation time and compatibility with rendering sofware are more important than a perfect explanation of the underlying scene, which this method achieves. The paper is structured as following: 1) The theory of this method is first describe and 2) we implement this on the GPU to allow real-time use. 3) A simulation with more advanced reflectance models is performed together with experiments in realistic scenes showing that we can estimate the light direction accurately to 20 degrees. 4) Examples of synthetic objects rendered realistically into real images are afterwards shown.

Methodology

To estimate the direction and location of a light source, several simplifying assumptions are made about the light source and how it interacts with objects in the scene. The **first assumption** is that the interaction between light source and object can be modelled by the

Lambertian reflectance model. This gives us the following equation:

$$I_o(\mathbf{p}) = \rho(\mathbf{p}) \min(\mathbf{n}(\mathbf{p})\mathbf{s}(\mathbf{p})^T i, 0) \tag{1}$$

According to the Lambertian reflectance model (Equation 1), the image intensity I_o at pixel $\mathbf{p} = \{x, y\}$ can be calculated given the albedo ρ, the surface normal $\mathbf{n}(\mathbf{p})$ of the object at $\mathbf{p}$ and the direction $\mathbf{s}(\mathbf{p})$ and intensity i of the light [1].

$$\mathbf{s}(\mathbf{p}) = \frac{\mathbf{l} - \mathbf{x}(\mathbf{p})}{||\mathbf{l} - \mathbf{x}(\mathbf{p})||} \tag{2}$$

where $\mathbf{l}$ is the light source position and $\mathbf{x}(\mathbf{p})$ is the 3D position of point $\mathbf{p}$ in the depth map. We assume that there is only a single dominant point light source present in the scene. The Kinect sensor gives the image intensities I and a 3D depth map. A small propotion of image intensity values do not have associated depth information (these image intensities are not used in our method). Given the 3D depth map, the surface normals $\mathbf{n}$ are computed using [27]. A schematic representation of our method is given in Figure 2 that shows the 3D depth map and the surface normals. The remaining unknown variables in the Lambertian Reflectance model are the albedo ρ and the direction $\mathbf{s}$ and intensity i of the light, making this equation still underdetermined. The **second assumption** is that the albedo of objects are similar in contiguous regions and that different albedo values on the same object are often easy to distinguish. Our methodology uses this assumption by using a colour-based

[1] for simplicity, we assume i is constant but real scene are affected by light attenuation of $\frac{1}{d^2}$ where d is the distance, in our experiment the effects of the lambertian equation where more dominant

segmentation method (Figure 2 shows an example of the segmentation), dividing the set of all image pixels P into contiguous segments (subsets) $P = \{R_1, ..., R_N\}$ that have a similar albedo ρ. Because the albedo is nearly constant in a segment, the albedo ρ at each pixel $\mathbf{p} \in R_j$ is estimated as the average albedo in that segment. This allows us to estimate the albedo in segment R_j (Equation 3) for an arbitary light source $\mathbf{s}_r(\mathbf{p}), i_r$.

$$\rho_{R_j} = \frac{1}{|R_j|} \sum_{\mathbf{p} \in R_j} \frac{I_o(\mathbf{p})}{\mathbf{n}(\mathbf{p})\mathbf{s}_r(\mathbf{p})^T i_r} \tag{3}$$

The main observation this paper uses is that *in the original image, a segment is likely to contain a gradient in the image intensity due to the light source position and the normals of the surface, while the albedo is similar for the entire segment*. By optimising the light source position, a better explanation of this intensity gradient can be found. We combine information from all segments R_j with $j = \{1, ..., N\}$ to obtain the full reconstructed image I_r. The light source position is determined by minimizing (Equation 5) the distance between the original intensity image I_o and the reconstructed image I_r (Equation 4).

$$I_r(\mathbf{p}) = \rho_{R_j} \min(\mathbf{n}(\mathbf{p})\mathbf{s}(\mathbf{p})^T i, 0), \mathbf{p} \in R_j \tag{4}$$

$$\{\mathbf{s}(\mathbf{p}), i\} = \arg \min_{\{\mathbf{s}(\mathbf{p}), i\}} \sum_{\mathbf{p} \in P} ||I_o(\mathbf{p}) - I_r(\mathbf{p})|| \tag{5}$$

We search for the light source position that reconstructs an image I_r (bottom-right panel in Figure 2) that is closest to the original image I_o (bottom-left). For these images only

intensity pixels with depth information are considered. The next section gives more details on the segmenation methods used to obtain the segments $R_1, ..., R_N$. The error function and the minimization strategies used to find the light source location are described in the next sections.

Segmentation

Segmentation (Figure 2, step b) is used to find regions that have approximately the same albedo, where we assume that the same image color implies the same albedo. In principle, any colour-based image segmentation method can be used to obtain the regions we consider to have the same albedo. Our experiments are performed using the colour-based segmentation method described in [28], where we remove segments that are smaller than $\lambda = 100$ pixels because they are often noisy and do not contain enough gradient information necessary for the minimization (Figure 2, step i). This segmentation method is however difficult to run in parallel and does not use the depth information from the Kinect sensor. More information about parallel segmentation is given in [29]. The depth information is not necessarily related to the albedo, but we assume depth discontinuities provide useful additional clues for object boundary segmentation. Therefore we include depth information when using the segmentation method of [28], computing distances in both colour and depth space. The GPU implementation for segmentation will be discussed later which also takes into account the depth information.

Error Function

In this section, we describe the error function E (Figure 2, step j) that is minimized (Figure 2, step i) to find the light position. The error function is the $L2$-norm between the original image intensity I_o and the reconstructed image intensity I_r (Equation 4), which can be minimized over parameters $(\mathbf{s}(\mathbf{p}), i)$ of the light source position:

$$E(\mathbf{s}(\mathbf{p}), i) = \sum_{\mathbf{p} \in P} ||I_o(\mathbf{p}) - I_r(\mathbf{p})|| \tag{6}$$

By using a reconstructed image, it is relatively easy to visually verify how well the observed scene can be explained by this method. To reconstruct the image I_r given the Lambertian model (Equation 4), the normals $\mathbf{n}$ and albedo ρ_{R_j} of the objects are needed together with the light direction $\mathbf{s}$ and light intensity i. From the depth map, we are able to compute the normal using [27]. In order to minimize the error function, the light source parameters $(\mathbf{s}_r, i_r)$ are the search parameters. The minimization method searches the $(\mathbf{s}_r, i_r)$ space to minimize Equation 6, leaving the albedo as the only unknown. Given an estimate of the parameters $(\mathbf{s}_r, i_r)$, the albedo ρ_r can be computed for every position $\mathbf{p}$ using the Lambertian equation:

$$\rho_r(\mathbf{p}) = \frac{I_o}{\mathbf{n}(\mathbf{p})\mathbf{s}_r(\mathbf{p})^T i_r} \tag{7}$$

Given the assumption that the albedo ρ_r of segment R_j is the same for all positions in the segment $\mathbf{p} \in R_j$, the albedo of the segment ρ_{R_j} can be estimated by taking the mean

or median ρ_r at all positions where the reflectance is larger than zero ($\mathbf{n}(\mathbf{p})\mathbf{s}_r(\mathbf{p})^T i_r > 0$). However, if the normals $\mathbf{n}$ are almost perpendicalur to the light direction $\mathbf{s}$, the albedo estimate becomes very unstable, which makes the median a better estimate for ρ_{R_j}.
However, the median is an expensive operation on the GPU. We address this by introducting a "robust mean", removing all albedo values above a certain threshold ($\tau = 2.5$), which gave experimentally better estimates than the normal mean and offers comparative accuracy performance to the median.

Notice that by estimating the albedo using the light source, the albedo varies inversely with the light intensity i_r. Therefore, the light intensity is arbitrarily set to $i_r = 1$.

Given the estimated albedo ρ_{R_j} for each segment, we can synthesise the entire reconstructed image I_r. In the case of an attached shadow pixel $\mathbf{p}$ ($\mathbf{n}(\mathbf{p})\mathbf{s}_r(\mathbf{p})^T i_r <= 0$), the synthesised image intensity values are set to zero. The difference between the reconstructed image I_r and the original image intensity I_o (see Equation 5) is then minimized by the method given in the next section
The error field $E()$ is visualized by computing the error function in a grid over the scene and interpolating the 3D grid values (Figure 3). The large white area shows that there is a global minimum in a position near the measured light position. It can be seen from Figure 3 that error values increase in a smooth fashion as the position moves further from the groundtruth.

Minimization

To find the light parameters, several search strategies can be used. In the previous section, we observed that albedo and intensity are related allowing us to set the light intensity ($i_r = 1$). In the case of a point light source, we can thus optimize over the variables (x, y, z-position of $\mathbf{l}$). Then, using the position of the light source, compute the light direction $\mathbf{s}(\mathbf{p})$ for every position $\mathbf{p}$. The light position can be found in most cases by using the downhill simplex method [30], because the error function is relatively smooth (see Figure 3). The viewpoint of the Kinect is used as the initial light source position, which allows an initial estimate of the albedo using Equation 7. The initial stepsize of the downhill simplex method to search for a point light source position $\mathbf{l}$ is 10 centimeters and the minimization will continue until convergence. For the GPU implementation, searching in a large grid of possible light source positions in parallel is easier because there are no dependencies in each iteration unlike with the downhill simplex method. The light position in the scene typically does not change which allows us to refine the grid search (i.e. by initializing based on previous interation's optimum) given the next frame, enabling us to determine the light position accurately within a couple of frames. However, our experiments are performed on only a single frame, where either the downhill simplex (CPU) or grid sampling (GPU) is used.

GPU implementation

Many works have taken advantage of massively parallel architectures like the GPU for obtaining interactive frame rates when doing point cloud processing. In [1] the main part of the algorithm is implemented on the GPU enabling a real-time 3D reconstruction and interaction with the environment using a moving depth camera like the Kinect. The authors in [31] leverage the computing power of the GPU to perform a textured 6 DoF (Degrees Of Freedom) reconstruction in real-time, performing the preprocessing and the main core of the algorithm on the GPU.

The main focus of this section is on the implementation of our light estimation algorithm and the extended GPU pipeline which is critical for enabling the estimation of the current light source position at interactive rates. Interactive frame rates also allow rendering realistic shadows in augmented reality scenes, thereby creating more realistic scenes.

Workflow

Most of the steps involved in the method are point-wise and therefore are well suited to be implemented on the GPU. While running this method on the CPU requires computing each point sequentially, the GPU performs the computation at many points in parallel, accelerating the execution time of each step considerably. In this case not only the processing of the point cloud is performed on the GPU, but also the pre-processing of the RGB-D map is performed on the GPU projecting the depth map obtained from the sensor to a point cloud.

Figure 4 shows the workflow for the GPU implementation from raw depth and color maps to estimated light source position. Each of these steps is executed in parallel on the GPU using the CUDA language [32] and the PCL (PointCloud Library) [33], which offers various algorithms and data structures for point cloud processing and visualization.

Preprocessing of Depth and Color Information

The first step to be performed on the raw depth map is an upsampling filtering technique [34] due to the noise present in the depth maps provided by the Kinect sensor. We used the traditional Bilateral Upsampling filter implemented on the GPU [35]. For every frame t obtained from the sensor, we launch as many CUDA threads as there are pixels in the depth map. Each CUDA thread computes in parallel a different pixel $\mathbf{p} = \{x, y\}$. After applying the denoising method each GPU thread projects a specific depth value to a 3D vertex in the camera's coordinate system using the intrinsic calibration parameters of the RGB-D sensor. This allows us to obtain an organized vertex map computed in parallel. Corresponding normal vectors for each vertex are also computed by each GPU thread by performing PCA over a local point neighbourhood in parallel. The normal vector is the outward facing Eigenvector with the smallest Eigenvalue.

The normal estimation is accelerated considerably on the GPU. Moreover, the normal estimation step takes advantage of the organized point cloud provided by the Kinect Sensor to perform a faster nearest neighbour (NN) search. Thanks to the organization of the point

cloud a fixed sized window can be used as the search space for NN search and thus considerably accelerate the normal estimation process. Running this algorithm on the CPU would not be able to provide real-time processing rates due to the complexity of the algorithm and the number of points that must be calculated sequentially.

Finally the RGB color map obtained from the Kinect sensor is also processed in parallel, performing color space conversion to the HSV space and then to grayscale. These two representations will be used later in the segmentation and light position estimation modules.

Segmentation

To achieve real-time performance using the GPU implementation the segmentation step has been adapted, so that it can be computed in parallel. As the initially proposed segmentation algorithm is iterative, for the GPU implementation we propose a hybrid approach capable of computing the segmentation partially on the GPU and afterwards computing the region extraction algorithm on the CPU. We extract patches of points with similar color, curvature and close proximity in Euclidean distance. The depth information previously obtained (and already hosted in the GPU memory) is used to aid the segmentation process.

The proposed algorithm uses the same approach as other region growing based algorithms [36, 37, 38], the main difference is the parallel computation of distances in different spaces using the pixel's neighbourhood and the use of all available information: Euclidean distances, curvature and colorimetric distances. The similarity function between pixels is

given by:

$$belongs_{region} = (||p - q|| \leq T_d) \wedge (|\overline{C_r} - C_q| \leq T_c) \wedge (|n_p \times n_q| \leq \cos \epsilon_{\theta_n}) \quad (8)$$

where $(||p - q|| \leq T_d)$ is a constraint based on the Euclidean distance between points p and q. T_d is obtained in real-time based on the point cloud resolution: the mean distance for each point p and its eight-neighbourhood k is calculated. Next, based on the average of these mean distances and the standard deviation, threshold T_d is given by: $T_d = \overline{d_k} + \sigma_d$, where $\overline{d_k}$ is the mean distance and σ_d is the standard deviation of all pre-computed distances. The established threshold for the maximum angle between two normal vectors is ϵ_{θ_n}. This is calculated in the same way as T_d, obtaining an angle threshold using the average of mean angles and the standard deviation. The target point will belong to the actual region if it is close in Euclidean space to the actual region and if the angle between normal vectors of both points are lower than an established threshold ϵ_{θ_n}. Furthermore, the colorimetric distance (in HSV) between the mean color $\overline{C_r}$ of the actual region R_a and the targeted point q is calculated, colorimetric distance is calculated using the following metric as discussed in [39]:

$$|\overline{C_r} - C_q| = [(s_r v_r \cos h_r - s_q v_q \cos h_q)^2 + (s_r v_r \sin h_r - s_q v_q \sin h_q)^2 + (v_r - v_q)^2]^{(\frac{1}{2})} \quad (9)$$

The proposed GPU segmentation algorithm takes advantage of the matrix organization in which the 3D points are stored, and the fact that they are already stored in the GPU mem-

ory. In this way, it is possible to calculate in parallel distances in Euclidean, curvature and colorimetric spaces for each point in the scene. Point distances are calculated relative to a point's direct neighbours in the vertical, horizontal and diagonal directions, resulting in eight distances for each pixel. The pre-computation of these distances on the GPU is then used in a region growing based segmentation using increasing distances in all spaces, deciding if neighbouring points must be added to the current region. This last step is performed on the CPU and uses all the precomputed distances in order to considerably accelerate this process. Furthermore, with the aim of removing the segments with a certain level of noise, segments with a number of points less than $\lambda = 100$ pixels, previously defined, are deleted.

The resulting implementation of this step yields a running time below 100ms allowing continuation with the next step on the GPU. This efficient version allows significantly lower runtimes compared to the CPU version and therefore the entire system is capable of running at interactive rates.

Figure 5 shows an example of the segmentation produced by the proposed GPU implementation. Results obtained are reasonably good, allowing the detection of regions in the scene with different color and geometric properties. Further results regarding the runtime and speed-up obtained compared with the CPU implementation are provided in the result sections.

Grid-based error minimization search

The algorithm for estimating the position of the light source in the scene is highly parallel. The different steps that are performed and how they are implemented on the GPU are described below.

Error estimation

Assuming a position of the point light source in the scene, it is necessary to calculate, for every point on each scene surface, the distance and direction vector from the scene point to this assumed light source position. This step is executed in parallel with one CUDA thread computing the Euclidean distance and the direction vector for each point. Using this data, we also compute the albedo factor for every point of the scene in parallel (Equation 7). Finally, using the extracted regions and the previously calculated albedo, the proposed error function (Equation 6) is computed.

Grid-base error minimization

To find the light source position with the minimum error, we perform a grid-based search (see Figure 6) in the scene calculating the error in different positions. The possible light source positions are distributed uniformly using a three-dimensional voxel grid (that forms a cube). The error function is computed in parallel in every voxel of the constructed grid. The GPU implementation of the error function allows us to perform this search in less than 1s for a grid of 125 uniform-size voxels with side length 1 meters.

Dynamic approach for error minimization over time

The estimated position of the light is refined every iteration t, where the position found in $t-1$ is used in t to re-estimate the albedo for the grid-base search error minimization. To improve position accuracy after every iteration the grid and its voxel size are decremented in successive frames by an established factor, here 0.75, until the position converges. We stop iterating (convergence) over this process when the voxel size is smaller than 10-15 centimetres (6 iterations considering an initial grid size of $4 \times 4 \times 4$ metres).

Simulation of Phong Reflectance model parameters

To estimate the illumination in a scene, certain assumptions have to be made about the scene. This work assumes that there is a single point light source present in the scene and surface appearance can be modelled by the Lambertian Reflectance model. For point light sources, the light direction $\mathbf{s}(\mathbf{p})$ is a vector from every position in the scene toward the position of the point light source. Most of the previous light source estimation approaches assume a directional light source[4, 5], however due to the Kinect depth map information it becomes possible to estimate also the location of the light source given that we have point light sources.

Light source localisations with more complex reflectance models is also possible. One of the important clues that a more complex reflectance model could use are specular reflections. Specular reflections are however different for each object making this a difficult clue to use.

In the case where a specular reflection model is used, an assumption has to be made about the specularity of the surface of each object (which involves setting multiple parameters in the Phong model).

In Figure 7, an experiment is performed with both the ambient and specular parameters of the Phong model by using OpenGL based rendering software. In this experiment, we look at the influence of both parameters on our estimation method, which only assume the diffuse term of the Phong model. The Phong model is given by:

$$I_o(\mathbf{p}) = \rho((\mathbf{p})(k_a i_a + k_d \min(\mathbf{n}(\mathbf{p})\mathbf{s}(\mathbf{p})^T, 0) i_d) + k_s \min(\mathbf{r}(\mathbf{p})\mathbf{v}(\mathbf{p})^T, 0)^\alpha i_s \quad (10)$$

$$\alpha \in |\mathcal{N}(10, 20)|, \beta \in |\mathcal{N}(0, 0.1)|, \gamma \in |\mathcal{N}(0, 0.1)|, \phi \in |\mathcal{N}(0, 0.1)| \quad (11)$$

$$k_a i_a = \frac{\beta}{(\beta + \gamma + \phi)}, \quad (12)$$

$$k_s i_s = \frac{\gamma}{(\beta + \gamma + \phi)}, \quad (13)$$

$$k_d i_d = \frac{\phi}{(\beta + \gamma + \phi)} \quad (14)$$

In Equation 10, k are the material properties determining the weight of ambient (a), diffuse (d) and specular (s) terms, i are the light source intensities with the same terms, $\mathbf{r}$ is the direction that perfectly reflects the ray of light given the light direction and the surface normal and $\mathbf{v}$ is the viewer direction. To investigate the effects of the ambient and specular terms on the method, we used the OpenGL rendering software where we added both specular and ambient parameters according to Equation 11-14 . This allows us to invesigate the effects these terms have on the light position. We rendered the scene 1000 times with

different frontal light positions and different parameters for α, β and γ. Examples are shown in Figure 7. We createe 1000 scens where the light source position varied and the teapot that random amount of specalur and ambient illumination components. A second 1000 had only the ambient component and no specular component and a third had no ambient component and only a specular component. By running only with the diffuse component, we get a perfect estimation of the light position, because there is no noise and segmentation given the simple scene perfect. Specular reflections are often present in only a small portion of the image and do not have a large influence on the estimates. Figure 7 shows that the light source location is estimated usually further away from the scene when ambient and specular light effects are present. From the experiments in which we varied only the ambient or specular parameters, it becomes clear that that ambient light has a larger effect on the estimate than specular reflections. It also shows that ambient light causes the estimated light source position to be estimated as further away from the scene, while specular reflectance will have the reverse effect. However taking both ambient and specular reflections into account is difficult because these material properties k vary for each object in the scene.

Another important clue that we currently do not make use of are cast shadows of known geometric objects: although the shadow positions can be calculated using triangulation and a ray tracer, this is a computationally expensive operation which would inhibit real-time performance for a potentially small increase in accuracy.

Experiments

Experimental Setup

To test the method, experiments are performed with different light sources and different scenes. To measure the accuracy of our method, we recorded several different scenes under different known illumination conditions. Most scenes are recorded with a single light source, which in our case is a 60 or 100 watts light bulb or a spotlight (see Figure 8). The distance between two salient control points in the scene on the ground plane are measured together with the height of the light source above the floor. Based on three hand-picked points in the Kinect data, we reconstruct the ground plane allowing us to determine the Kinect co-ordinates for the true light source position. These positions are used as Groundtruth in our experiments to evaluate the performance of estimating the light source position and angle. Some of the scenes that have been captured with the Kinect are shown in Figure 9. For most scenes, we made multiple captures under different illumination conditions. This dataset is available at http://www.dtic.ua.es/jgpu12/lightEstimation/ (password: lightEstimationEdi).

Measurement

To measure the accuracy of our method, the difference in the **angle** between the estimated position and the measured position is calculated. Angle comparison is performed by measuring for every pixel (with related 3D position) in the scene “the angle between the measured

light source and the estimated light source". For the rendering of objects, having the angle correct seems to be the most important component. In the scene, we can also measure the **distance** between the estimated and the measured position of the light source. This is however deemed less important than the angle. For instance, the spotlight light source is not exactly a point light source so it is often estimated with a low angle error but at a distance from the scene larger than the measured light source. The **speed (ms)** of the algorithm is the final measure, where we compare a CPU implementation with several GPU implementations.

Accuracy Results

Figure 9 shows some of the recorded scenes together with the estimated and measured light positions. Our dataset consists of 23 different recordings of 6 different scenes illuminated with different light sources. The two scenes in the top rows in Figure 9 show the potential of this method for estimating the light source position and angle. Determining the position accurately seems to be difficult, while the angle is often correct which is more important for rendering objects realistically in the scene. The scene at the bottom of Figure 9 has a large difference in angle and distance between the estimated and measured light position. The main reason for the large difference seems to be the segmentation, which segments multiple objects with different albedo as one object. In our observations, the segmentation is often the main cause of errors, because it sometimes segments multiple objects with different albedos

incorrectly, and therefore assumes these objects have the same albedo, which causes errors in the reconstructed image.

In the theory above different alternatives were proposed for computing the albedo (using mean, robust mean or median). These alternatives have implications on the speed of the method. In this section, we compare the different alternatives for the computation of the albedo, search method and segmentation method. Our default method for the computation of the albedo is the median, for search the default is the downhill simplex method and for segmentation it is the Graph-Based Image Segmetation where the only variable parameter K = 200, where a larger value of K creates larger image segments

Computation of the Albedo: We suggest using the mean, robust mean or median in order to compute the albedo of a segment. In Figure 10, the accuracy in distance and difference in angles is shown averaged over all scenes. The distance computed using the median has a large standard devation. It is especially difficult to perform accurately for scenes with a large distance to the light source or scenes with spotlights. Figure 10 shows that the angle is much more accurate for the median than the mean, which is more important for this application. However, the median is a more expensive operation on the GPU, because it applies a sort over the entire set of values. Because of this, we experimented with a robust mean, removing all albedo values above a certain threshold ($\tau = 2.5$), which gives better estimates than the normal mean and offers comparative accuracy performance to the median (Figure 10) while using athe computationally cheaper mean operation.

Search Methods: Two search methods are used for finding the light position, namely a grid search on the GPU and the downhill simplex method on the CPU. Although the grid size can be set in our software, for the experiments a grid from the Kinect sensor of -2 metres to 2 metres is used. A comparison between the downhill simplex method and the grid search is given in Figure 11. The downhill simplex method performs slightly worse than the grid search, however the grid search seems to have a larger variance, which seems to be mainly due to mistakes in the segmentation allowing multiple illumination explanations to be likely for a scene.

Segmentation Methods: The segmentation methods are different between the CPU and GPU. On the CPU, the Graph-Based Image Segmentation [28] is performed both with only the image and on both image and depth information with two parameter settings (K = 100 and K = 200) where a large value of K creates larger albedo segments. On the GPU, a different segmentation method is used on both the image and depth information. A comparison of these methods is given in Figure 11, where the median performance of the different segmentation methods is very similar. The depth information makes the median angle slightly better but also has a larger standard devation. The GPU implementation of the segmentation, which is not Graph-Based but uses region growing gives very similar results to the CPU implementations, which shows that our method does not depend on a single segmentation methodology.

Performance (ms)

The GPU version of the proposed method has been tested on a desktop machine with an Intel Core i3 540 3.07Ghz and different CUDA capable devices. The GPU implementation was first developed on a laptop machine equipped with an Intel Core i5 3210M 2.5 Ghz and a CUDA compatible GPU. Table 1 shows different models that have been used and their main features. We used different models ranging from the integrated GPU on a laptop to a more advanced model, demonstrating that the GPU implementation can be executed on different GPUs and obtains good runtimes on all systems experimented with.

The performance obtained by the GPU implementation allow us to executed the proposed method faster than 1 sec. In Table 2 we can see the different steps that have been accelerated using the GPU and their different runtime and the speed-ups achieved for the different graphics boards. The obtained acceleration is relative to a CPU implementation of the proposed method.

The best performance was obtained with the graphics board with the largest number of CUDA cores (GTX480) and the largest memory bandwidth, performing $\sim 6-7\times$ faster than the CPU implementation. This allows our light source position estimation technique to be used for demanding realistic rendering applications in real-time.

The overall speed-up is not so high compared to other steps because although the light estimation process itself is parallelized at pixel level, we still have to traverse all voxels in the grid and estimate the light position in each voxel (brute-force). A more complex approach

could be developed overlapping the computation in parallel over different voxels (task parallelism). We discarded this approach because in experiments we obtained full occupancy of GPU processors with the current implementation, so this high level of parallelism would need more powerful GPUs.

Another interesting aspect of the results shown in Table 2 is that the GPU implementation allows us to compute operations that are prohibitively slow on the CPU such as normal estimation using PCA and the depth map noise reduction using bilateral filtering.

Rendering a Synthetic Object into the Scene

Technical Details

By estimating the light source position, we are able to realistically render a new object (see Figure 12) into each RGB image created by the Kinect, such that the new object appears natural in terms of lighting, shading and shadows. To do this, we first create an approximate surface over the coloured depth data using [40]. This surface gives us the geometry of the scene. In order to render the new object, we first use this geometry to design a non-penetrating motion for the object using keyframe animation in Autodesk Maya. Using the light position and properties estimated by our method, we can create a point light element in Maya. This light position is already in the aligned camera space, so no additional calculation needs to be performed on the light location. A virtual camera that matches the Kinect's

properties is created, using the specifications provided at [41]. The important values for us were horizontal field of view and film aspect ratio. These were set to 62.7 degrees and 1.33 respectively. In order to keep the camera model simple, we did not apply any depth-of-field or motion blurring effects. For rendering the artificial images, we used the NVIDIA Mental Ray raytracing system [42]. We rendered a separate shadow pass, where only the shadows on the background surface (that we generated from the depth data) and on the inserted objects were calculated. This results in a 640x480 render where non-transparent colours are the values to remove from the unshadowed image. Self-shadowing is disabled for the background geometry in order to prevent the duplication of shadows in the final image. We then rendered an unshadowed pass using the light positions, with only the new character or object visible. For this reason we call this second pass the character render. Using these two renders we can finally composite the character render, the shadow render and the original RGB image from the Kinect together to create the final image. We used the "replace" blend mode for the character render over the original Kinect image, and the "subtract" blend mode for the shadows on top of these two. Using the subtract mode allows us to use the original colour data from the Kinect, whilst computing the shadow effect for each pixel per frame, giving us realistic shadows that depend only on the quality of the reconstructed geometry.

Resulting scenes

In Figure 12, two rendered scenes are shown where we used both the measured groundtruth position (middle scene) and the estimated position (right scene). It is clearly visible that the shadows from the augmented object rendered in both scenes are different, however without any more knowledge of which scene is rendered using the measured light position, it is hard to tell which object is rendered with the correct illuminant. Although the estimation of the light source will never be entirely accurate, with these scenes we show that a reasonable estimation is often sufficient. The experience of having objects that are rendered whilst taking into account the illumination information in the scene will in most cases be enough. In Figures 13 and 14, other synthetic objects are rendered into the scene to show the potential of this method. In the supplemental materials videos are included showing that the object can interact with the scene. Although this material is developed offline, given the speed of our methodology we should also be able to connect these methods to augmented reality software in the future. Figure 13 shows that the shadows interact with the environment, showing that the shadows take into account the mesh of the background objects. Figure 14 shows that you can replace objects or people, although this was done offline. Using object segmentation this can also be done online.

Discussion

In this paper, a method for estimating the light source position is described for the application of rendering synthetic objects in a scene. A new method for estimating the light source position based on 3D depth data with a registered colour image (e.g. given by a Kinect sensor) has been developed. We show that this estimation can be performed at speeds on the order of once per second with our GPU implementation. Often both the Kinect position and light source position do not change much over time, which makes this implementation useful for the application of augmented reality. We verified our method using both OpenGL rendering software and with a dataset of real scenes with measured light position. The experiments show that the angle of the light source can be estimated with an average error of 20 degrees between measured and estimated light source positions. These light source estimates are good enough for rendering synthetic objects into the scene with realistic looking illumination conditions.

Although this work is limited to the estimation of a single point light source, we noticed that this simple assumption often also works in scenes with more difficult illumination conditions like fluorescent tubes, reconstructing an image that explains the scene as well as possible. Although the Kinect is not often used in outdoor environments, estimating directional light sources like the sun should be possible by checking if the distance of the light source to the scene becomes very large and checking if a directional light source in the same direction is able to give a better minimization of the error function. The minimization proce-

dure can also be extended to search for multiple light sources, however this adds complexity to the minimization, making it less attractive for augmented reality. Future work can focus on other applications where illumination estimation is important, like improving 3D surface using shape from shading or creating illumination invariant features for scene recognition.

Acknowledgment

This work is partially supported by the Fish4Knowledge project, which is funded by the European Union 7th Framework Programme [FP7/2007-2013], by the HiPEAC Network of Excellence, by Valencian Government grant BEFPI/2012/056 and by EPSRC (EP/P504902/1, EP/H012338/1)

References

[1] Shahram Izadi, Richard A. Newcombe, David Kim, Otmar Hilliges, David Molyneaux, Steve Hodges, Pushmeet Kohli, Jamie Shotton, Andrew J. Davison, and Andrew W. Fitzgibbon. Kinectfusion: real-time dynamic 3d surface reconstruction and interaction. In *SIGGRAPH Talks*, pages 23:1–23:1, 2011.

[2] Richard A. Newcombe, Shahram Izadi, Otmar Hilliges, David Molyneaux, David Kim, Andrew J. Davison, Pushmeet Kohli, Jamie Shotton, Steve Hodges, and Andrew W.

Fitzgibbon. Kinectfusion: Real-time dense surface mapping and tracking. In *ISMAR*, pages 127–136, 2011.

[3] Bastiaan J. Boom, Sergio Orts-Escolano, Xin X. Ning, Steven McDonagh, Peter Sandilands, and Robert B. Fisher. Point light source estimation based on scenes recorded by a rgb-d camera. In *British Machine Vision Conference*, 2013.

[4] Yang Wang and Dimitris Samaras. Estimation of multiple directional light sources for synthesis of mixed reality images. In *Proceedings of the 10th Pacific Conference on Computer Graphics and Applications*, PG '02, pages 38–47, Washington, DC, USA, 2002. IEEE Computer Society.

[5] Yang Wang and Dimitris Samaras. Estimation of multiple directional light sources for synthesis of augmented reality images. volume 65, pages 185–205, July 2003.

[6] Yuanzhen Li, S. Lin, Hanqing Lu, and Heung-Yeung Shum. Multiple-cue illumination estimation in textured scenes. In *Computer Vision, 2003. Proceedings. Ninth IEEE International Conference on*, pages 1366 –1373 vol.2, oct. 2003.

[7] Kenji Hara, Ko Nishino, and Katsushi Ikeuchi. Light source position and reflectance estimation from a single view without the distant illumination assumption. *IEEE Trans. Pattern Anal. Mach. Intell.*, 27(4):493–505, April 2005.

[8] Wei Zhou and Chandra Kambhamettu. Estimation of the size and location of multiple area light sources. In *Proceedings of the Pattern Recognition, 17th International Con-*

ference on (ICPR'04) Volume 3 - Volume 03, ICPR '04, pages 214–217, Washington, DC, USA, 2004. IEEE Computer Society.

[9] Wei Zhou and Chandra Kambhamettu. A unified framework for scene illuminant estimation. *Image Vision Comput.*, 26(3):415–429, March 2008.

[10] Paul Debevec. Rendering synthetic objects into real scenes: bridging traditional and image-based graphics with global illumination and high dynamic range photography. In *Proceedings of the 25th annual conference on Computer graphics and interactive techniques*, SIGGRAPH '98, pages 189–198, New York, NY, USA, 1998. ACM.

[11] S. Gibson, T.L.J. Howard, and R.J. Hubbold. Image-based photometric reconstruction for mixed reality. In *SIGGRAPH 2001 Sketches and Applications Program*, August 2001.

[12] Kusuma Agusanto, Li Li, Zhu Chuangui, and Ng Wan Sing. Photorealistic rendering for augmented reality using environment illumination. In *Proceedings of the 2nd IEEE/ACM International Symposium on Mixed and Augmented Reality*, ISMAR '03, pages 208–216, Washington, DC, USA, 2003. IEEE Computer Society.

[13] S. Heymann, A. Smolic, K. Müller, and B. Froehlich. Illumination reconstruction from real-time video for interactive augmented reality. In *International Conference on Video and Image Processing*, 2005.

[14] Steven D. Hordley. Scene illuminant estimation: Past, present, and future. *Color Research & Application*, 31(4):303–314, 2006.

[15] A. Gijsenij, T. Gevers, and J. van de Weijer. Computational color constancy: Survey and experiments. *Image Processing, IEEE Transactions on*, 20(9):2475 –2489, sept. 2011.

[16] Yanli Liu, Xueying Qin, Songhua Xu, Eihachiro Nakamae, and Qunsheng Peng. Light source estimation of outdoor scenes for mixed reality. *Vis. Comput.*, 25(5-7):637–646, April 2009.

[17] Jean-Franois Lalonde, Alexei A. Efros, and Srinivasa G. Narasimhan. Estimating the natural illumination conditions from a single outdoor image. *International Journal of Computer Vision*, 98:123–145, 2012.

[18] Yanli Liu and Xavier Granier. Online tracking of outdoor lighting variations for augmented reality with moving cameras. *IEEE Transactions on Visualization and Computer Graphics*, 18:573–580, 2012.

[19] Claus B. Madsen and Michael Nielsen. Towards probe-less augmented reality - a position paper. In *GRAPP*, pages 255–261, 2008.

[20] Claus B. Madsen and Brajesh Behari Lal. *Probeless Illumination Estimation for Outdoor Augmented Reality*. INTECH, 2010.

[21] Imari Sato, Yoichi Sato, and Katsushi Ikeuchi. Illumination from shadows. *IEEE Trans. Pattern Anal. Mach. Intell.*, 25(3):290–300, March 2003.

[22] A. Panagopoulos, T.F.Y. Vicente, and D. Samaras. Illumination estimation from shadow borders. In *Computer Vision Workshops (ICCV Workshops), 2011 IEEE International Conference on*, pages 798 –805, nov. 2011.

[23] J. Frahm, K. Koeser, D. Grest, and R. Koch. Markerless augmented reality with light source estimation for direct illumination. In *Visual Media Production, 2005. CVMP 2005. The 2nd IEE European Conference on*, pages 211 – 220, 2005.

[24] Jonathan T Barron and Jitendra Malik. Intrinsic scene properties from a single rgb-d image. *CVPR*, 2013.

[25] Qifeng Chen and V. Koltun. A simple model for intrinsic image decomposition with depth cues. In *Computer Vision (ICCV), 2013 IEEE International Conference on*, pages 241–248, Dec 2013.

[26] L.-F. Yu, S.-K. Yeung, Y.-W. Tai, and S. Lin. Shading-based shape refinement of rgb-d images. In *IEEE Conference on Computer Vision and Pattern Recognition (CVPR)*, 2013.

[27] Toby. P. Breckon and Robert. B. Fisher. Environment authentication through 3d structural analysis. In *Image Analysis and Recognition*, volume 3211 of *Lecture Notes in Computer Science*, pages 680–687. Springer Berlin Heidelberg, 2004.

[28] Pedro F. Felzenszwalb and Daniel P. Huttenlocher. Efficient graph-based image segmentation. *Int. J. Comput. Vision*, 59(2):167–181, September 2004.

[29] Jan Wassenberg, Wolfgang Middelmann, and Peter Sanders. An efficient parallel algorithm for graph-based image segmentation. In *Proceedings of the 13th International Conference on Computer Analysis of Images and Patterns*, CAIP '09, pages 1003–1010, Berlin, Heidelberg, 2009. Springer-Verlag.

[30] J. A. Nelder and R. Mead. A simplex method for function minimization. *The Computer Journal*, 7(4):308–313, 1965.

[31] Dominik Neumann, Felix Lugauer, Sebastian Bauer, Jakob Wasza, and Joachim Hornegger. Real-time RGB-D mapping and 3-D modeling on the GPU using the random ball cover data structure. In *ICCV Workshops*, pages 1161–1167. IEEE, 2011.

[32] NVIDIA. *NVIDIA CUDA Programming Guide 4.2*. 2008.

[33] Radu Bogdan Rusu and Steve Cousins. 3D is here: Point Cloud Library (PCL). In *Proceedings of the IEEE International Conference on Robotics and Automation (ICRA)*, Shanghai, China, May 9-13 2011.

[34] C. Tomasi and R. Manduchi. Bilateral filtering for gray and color images. In *Proceedings of the Sixth International Conference on Computer Vision*, ICCV '98, pages 839–846, Washington, DC, USA, 1998. IEEE Computer Society.

[35] Derek Chan, Hylke Buisman, Christian Theobalt, and Sebastian Thrun. A Noise-Aware Filter for Real-Time Depth Upsampling. In *Workshop on Multi-camera and Multi-modal Sensor Fusion Algorithms and Applications - M2SFA2 2008*, Marseille, France, 2008.

[36] Yinghui Xiao Qingming Zhan, Yubin Liang. Color-based segmentation of point clouds. In *ISPRS Volume XXXVIII-3/W8*, 2009.

[37] Dirk Holz and Sven Behnke. Fast range image segmentation and smoothing using approximate surface reconstruction and region growing. In *Proceedings of the 12th International Conference on Intelligent Autonomous Systems (IAS)*, Jeju Island, Korea, June 2012.

[38] T. Rabbani, F. A. van den Heuvel, and G. Vosselmann. Segmentation of point clouds using smoothness constraint. In *IEVM06*, 2006.

[39] James D. Foley, Andries van Dam, Steven K. Feiner, and John F. Hughes. *Computer graphics: principles and practice (2nd ed.)*. Addison-Wesley Longman Publishing Co., Inc., Boston, MA, USA, 1990.

[40] Michael Kazhdan, Matthew Bolitho, and Hugues Hoppe. Poisson surface reconstruction. In *Proceedings of the fourth Eurographics symposium on Geometry processing*, SGP '06, pages 61–70, Aire-la-Ville, Switzerland, Switzerland, 2006. Eurographics Association.

[41] Kurt Konolige and Patrick Mihelich. Technical description of kinect calibration. http://www.ros.org/wiki/kinect_calibration/technical.

[42] NVIDIA. Mental ray: Rendering imagination visible. http://www.mentalimages.com/products/mental-ray.html.

Bastiaan J. Boom received his bachelor engineering degree in Computer Science from the Hogeschool van Amsterdam in 2002 and a the Master degree from the Free University Amsterdam in Computer Science in 2005 He has a PhD degree from the University of Twente (2010), where he specialised in the fields of biometrics. He was Research Associated at the University of Edinburgh and is currently working for Disney Research, where his research interests are in computer vision and related topics.

Sergio Orts-Escolano received his B.Sc and M.Sc in Computer Science from the University of Alicante (Spain) in 2010 and 2011 respectively. He is currently a researcher with the Department of Computer Technology at the University of Alicante. His research interests include 3D vision, surveillance systems, parallel computing on GPUs and neural networks.

Xin Xin Ning received his M.Sc (Hons) degreein Computer Science from the University of Edinburgh in 2012. Currently, he is studying at the Entertainment Technology Center at Carnegie Mellon University.

Steven McDonagh received the BSc degree in Computer Science and Artificial Intelligence from The University of Edinburgh in 2008. He is currently a PhD candidate in the School of Informatics, University of Edinburgh. His interests span a variety of topics in computer vision, image processing and machine learning. His current work focuses on the analysis and implementation of multi-view

registration algorithms, range data processing and geometric modelling.

Peter Sandilands studied for the Ph.D. under Dr. Taku Komura at the School of Informatics in the University of Edinburgh, previously receiving his BSc (Hons) in Artificial Intelligence and Computer Science from the same institution. In 2010, he won the ScotlandIS Young Software Engineer of the Year award for his work on visual and auditory systems of the Sony AIBO and in 2012 won Best Student Paper at the Motion in Games conference. His current research focus is on capture and generation of close interactions between actors and objects. He now works in industry for Rockstar North.

Prof. Robert B. Fisher received a B.S. with Honors (Mathematics) from California Institute of Technology (1974) and a M.S. (Computer Science) from Stanford University (1978). He received his PhD from University of Edinburgh (1987), investigating computer vision. Since then, Bob has been an academic at Edinburgh University, now in the School of Informatics, where helped found the Institute of Perception, Action and Behaviour.

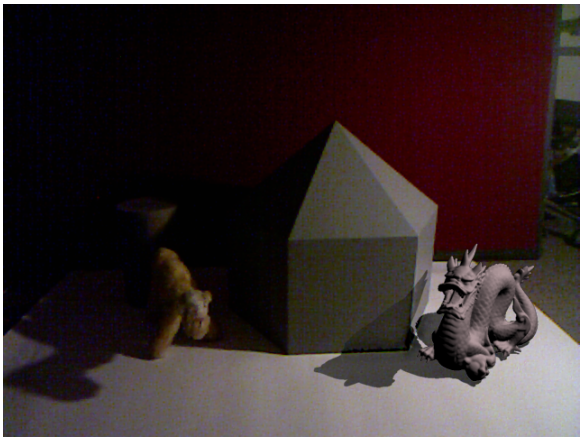

Figure 1: A synthetic object (dragon, right) that is rendered into a real-world scene recorded with the Kinect, where the illumination of the synthetic object is similar to the scene and the rendered shadows take into account geometry of the scene based on an estimated light source position determined using only the intensity image and depth information.

Device Model	**CUDA cores**	**Global Mem**	**Bandwidth Mem**
Quadro 2k	192	1 GB	41.6 GB/s
GeForce GTX 480	480	1.5 GB	177.4 GB/s
GeForce GT630M	96	1 GB	32 GB/s

Table 1: CUDA capable devices used in experiments.

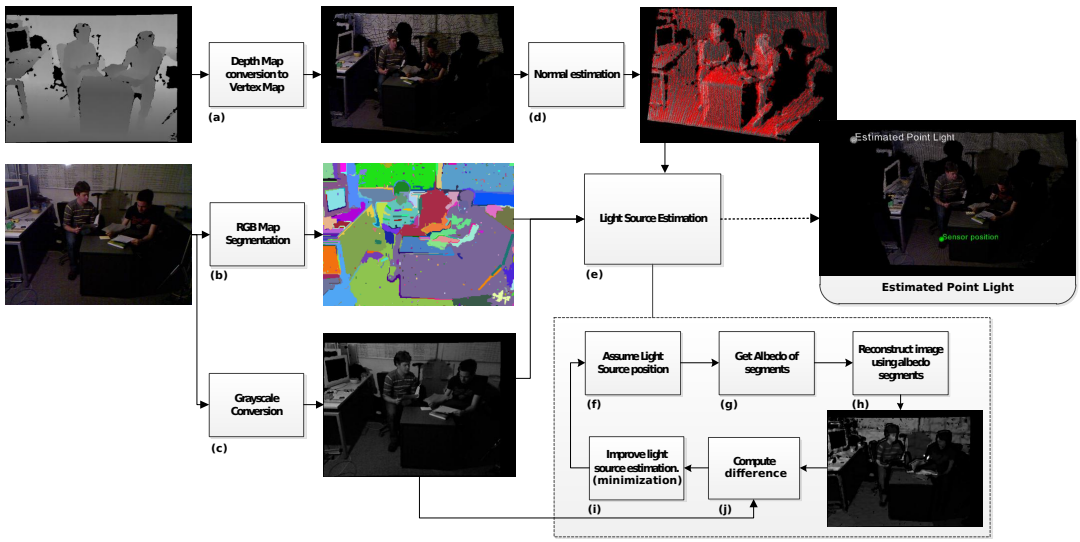

Figure 2: A schematic representation of the method to estimate the light source position, where given the input (depth map and image shown left), we compute the normals (top-right) and segments (middle). Afterwards we search for the light source position that gives the best reconstructed image (bottom-right) by minimizing the distance with the original image (bottom-middle), allowing us to find the light source direction shown in (middle-right). The method in box e is expanded to show the contained submethods (boxes f to j)

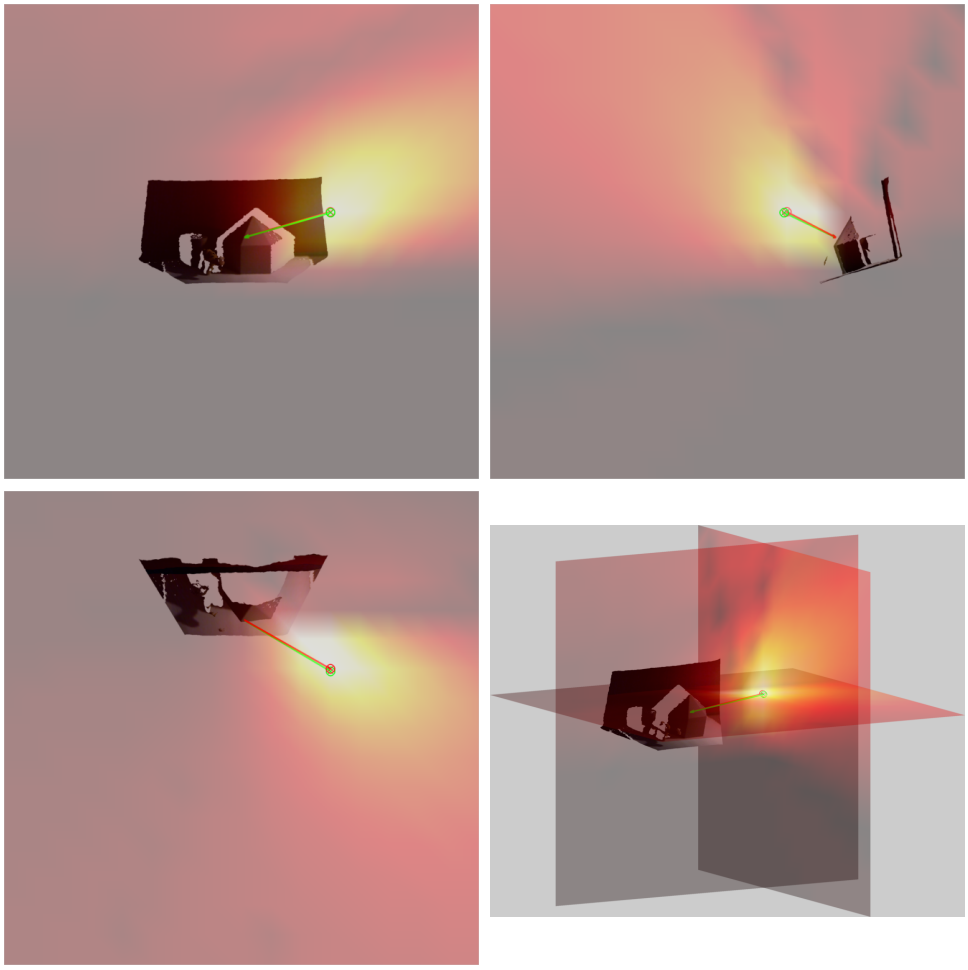

Figure 3: The error function given an example point light source is shown, where the scene is shown from different angles (The brighter the value, the smaller the error. For visualization, the error is computed in a 3D grid of -2 to 2 meters with steps of $\frac{1}{4}$ meters, where interpolation is used to plot the error values shown in the grid slices. The obtained error field is smooth allowing us to use simple minimization strategies. The minimum is located close to the true light position (green dot) and the error function seems to have a single minima, which is the desired behavour given that the estimated light source direct is important. The red vector represents the line from the error function minima to the centroid of the RGB-D scene data and the green vector gives the measured lin from the groundtruth light position to the centroid of the RGB-D scene data.

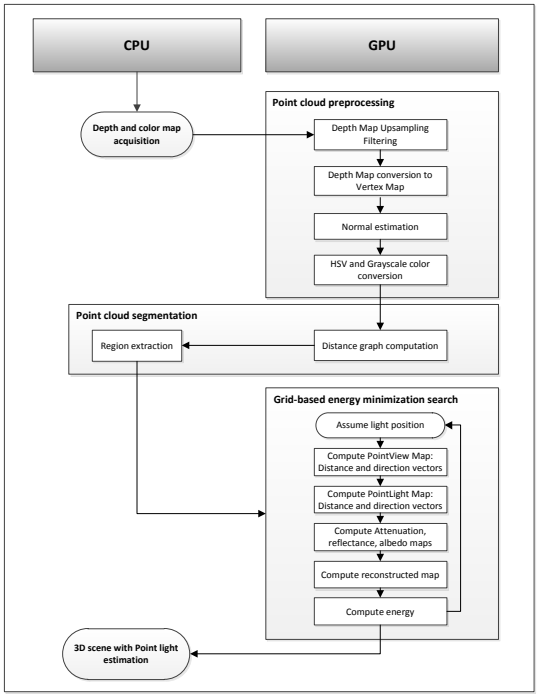

Figure 4: Extended work flow diagram for computing the Light Source Position Estimation algorithm on the GPU. Note that most of the steps have been moved to the GPU in order to achieve a runtime faster than 1s on an off-the-shelf consumer GPU.

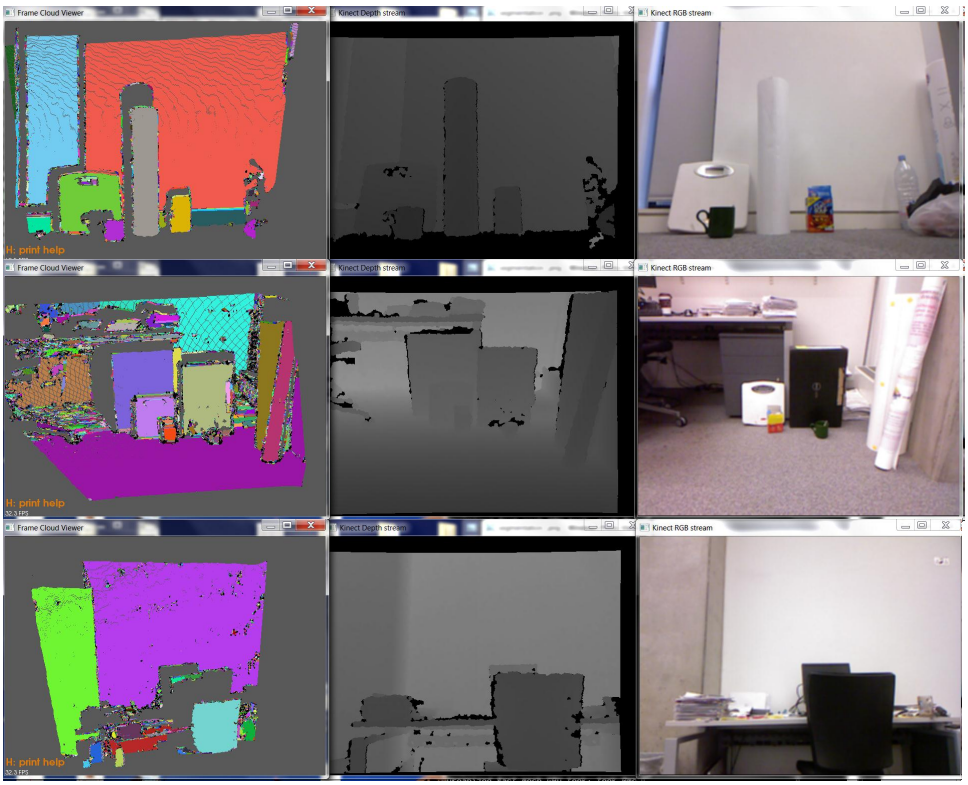

Figure 5: Point cloud segmentation examples. Left column: Segmented point cloud. Center column: Depth map. Right column: Color map smoothed using bilateral filtering. Segmentation results are satisfactory allowing real-time scene region extraction.

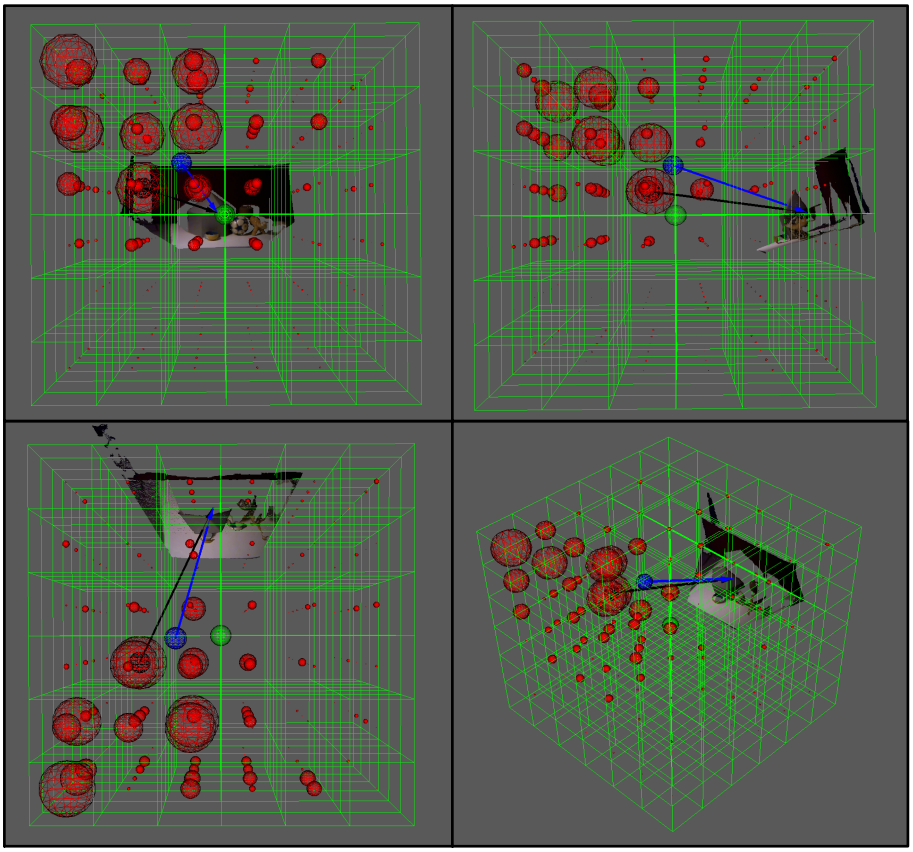

Figure 6: The error function given a point light source is shown, where the scene is shown from different angles. The green sphere is the camera position, while the blue sphere is the measured position of the light source with a blue arrow toward the middle of scene. In this figure, the error is computed in a grid of -2 to 2 meters with steps of $\frac{2}{3}$ meters. The red sphere are the points whre teh errors are sampled and the sphere is inversely proportional to the error for visualization purposes. The largest red sphere shows the minimum error where black arrow is the global minimum direction for this grid, which is very close to the measured light position.

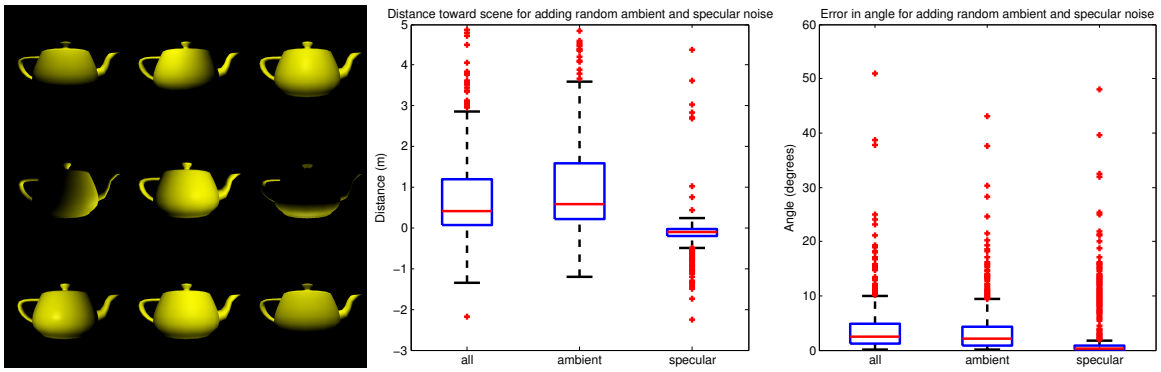

Figure 7: Rendering a teapot 1000 times with the light source at different positions and under different values of the "ambient" and "specular" parameters in the Phong model (examples are shown at the left). The middle boxplot shows the Euclidean distance error in world coordinate between the estimated and true lightsource positions, where a negative distance means the estimated light source position is closer to the scene than the true light source position. The right boxplot shows the difference in angle between the estimated and true light position with respect to the center of the scene. This experiment shows that the ambient parameter has a much larger effect on both the estimated distance and angle than the specular reflection parameter. Specular reflections cause the light position to be estimated slightly closer to the scene while the ambient parameter has the reverse effect.

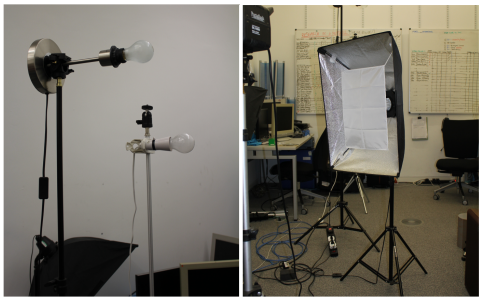

Figure 8: The light sources used to record all the scenes, the left photo show the 60 and 100 watt light bulbs. The right photo show the spotlight.

Step	GT630M	GTX480	Quadro2k	CPU	GT630M	GT480	Quadro2k
Bilateral filtering of depth map	11 ms	**5 ms**	8 ms	1008 ms	91.63x	**201.6x**	126x
Point cloud projection	2 ms	**1 ms**	1 ms	50 ms	25x	**50x**	50x
Normal estimation	9 ms	**1 ms**	8 ms	190 ms	21.11x	**190x**	23.75x
Compute distances graph for segmentation	13 ms	**4 ms**	11 ms	101 ms	7.76x	**25.25x**	9.18x
Compute cloud resolution	7 ms	**4 ms**	6 ms	330 ms	47.14x	**82.5x**	55x
Compute error given point light source	10 ms	**9 ms**	12 ms	50 ms	5x	**5.55x**	4.16x
Grid-based error minimization	595 ms	**583** ms	818 ms	3056 ms	5.13x	**5.24x**	3.73x
Total execution time	778 ms	**718 ms**	958 ms	4855 ms	6.24x	**6.86x**	5.06x

Table 2: Runtime comparison and speed-up obtained for the proposed method using different graphics boards. The fastest runtime was achieved by the graphics board NVIDIA GTX480 running the algorithm 6.86 times faster than on a conventional CPU.

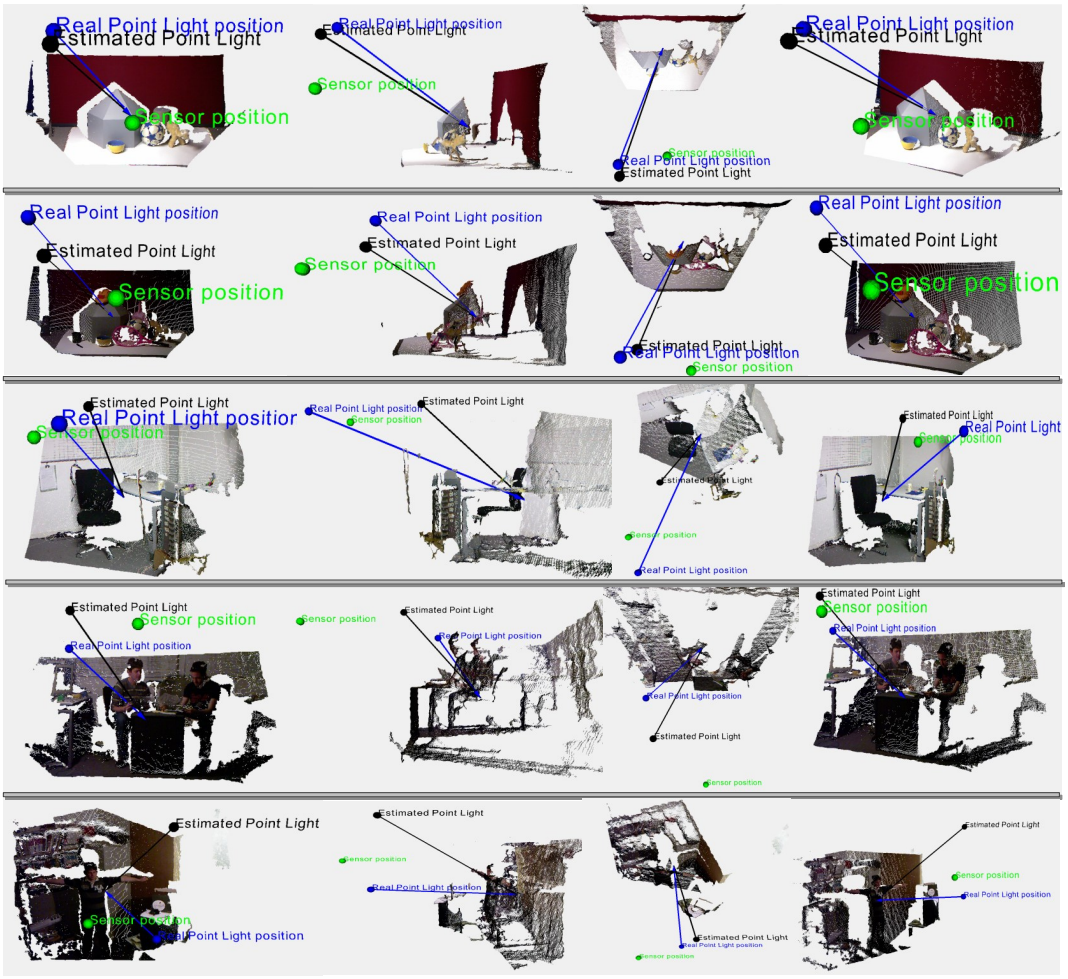

Figure 9: Five different scenes (one scene per row) of our dataset together with the camera position (green ball) and the estimated (black ball) and measured (blue ball) light position. Each row contains different views of one scene. These scenes are shown from different angles in order to visualize the 3D position or the light sources correctly. The estimation of the light source position of the first scenes are very accurate, however the last scene shows that the accuracy of more complex scenes can be more challenging. The rendering using the estimated light source position in this scene (Figure 14) still looks realistic.

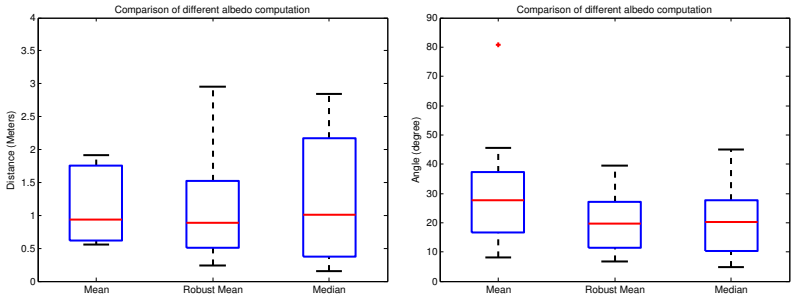

Figure 10: The boxplot of the error in distance and angle between the measured and estimated light source position, for computing the albedo using the mean, robust mean, median. These are obtained from our dataset of 23 different recordings on 6 different scenes.

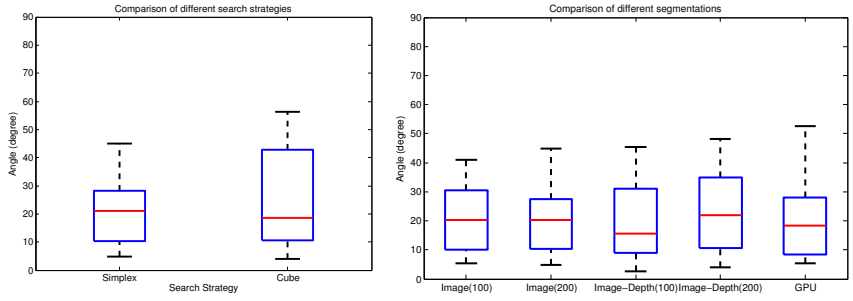

Figure 11: The boxplot of the error in angle between the measured and estimated light source position, left: using different search strategies, right: using different segmentation methods. These are obtained from our dataset of 23 different recordings on 6 different scenes.

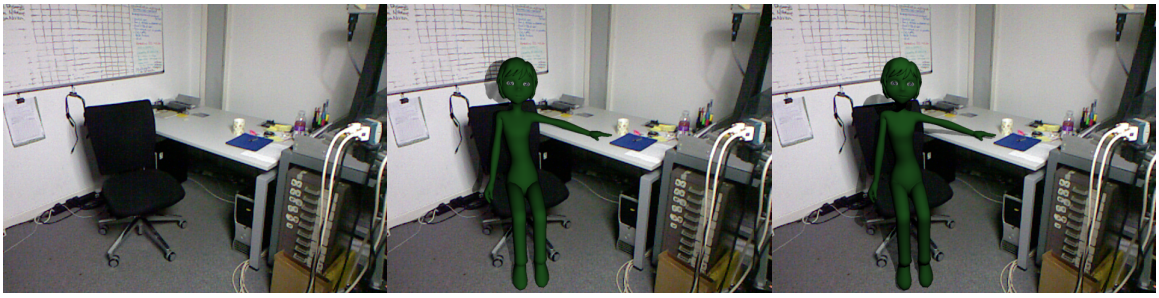

Figure 12: The rendering of a object in the scene is shown. The left image is the original image, the middle image is rendered using the measured light position and the right image obtained with the estimated light position. Although the shadows are clearly different, it is difficult for humans to observed what the correct light position was given the small differences in angle.

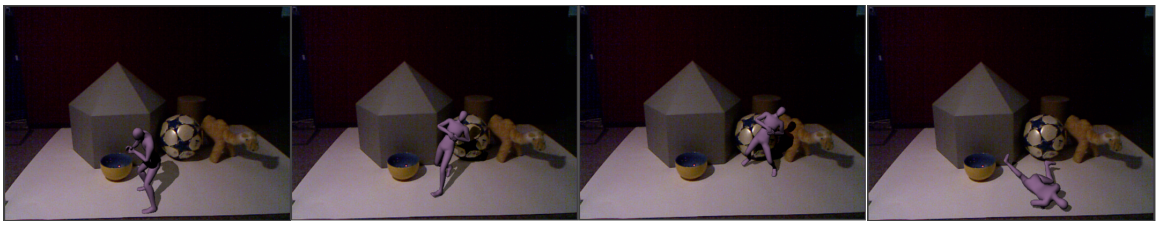

Figure 13: Multiple frames of a virtual object (character) rendered into the scene showing the interaction between the shadows of the inserted character and the background objects.

Figure 14: Replacing the person in the scene with a virtual character, by taking into account the lighting of the scene (can you spot the second addition?).